REGULAR PAPER

Analysis of Optical OAM Mode Conversion Using Elastic Vortex Wave in Graded Index Optical Fiber

Takuya Shoro[1], Hiroki Kishikawa [1]*, Nobuo Goto[1]

[1]*Department of Optical Science, Graduate School of Science and Technology, Tokushima University, Tokushima 770-8506, Japan*

We theoretically analyze acousto-optic (AO) mode conversion between optical orbital angular momentum (OAM) modes using an elastic vortex wave (EVW) carrying OAM in a squared graded index (GI) fiber. The AO mode conversion from the fundamental mode to the higher order optical OAM mode is a useful technology to generate optical OAM modes in the GI fiber. This paper clarify the contribution of each component of the dielectric constant perturbation caused by the EVW to the AO mode conversion.

1. Introduction

To meet the growing demand of the communication traffic, the optical transmission technology has continuously employed various multiplexing techniques such as time division multiplexing (TDM), wavelength division multiplexing (WDM), optical code division multiplexing (OCDM), polarization division multiplexing (PDM), and space division multiplexing (SDM). Orbital angular momentum (OAM) has been attracting much attentions as a novel degree of multiplexing since it is one of the orthogonal modal basis for mode division multiplexing (MDM) which is a special case of SDM. Using multiple OAM states potentially increases the transmission capacity[1] due to the fact that different azimuthal OAM modes are mutually orthogonal while propagating coaxially.[2–4] An OAM beam has a spiral phase front and donut shape intensity distribution. This unique structure produces a variety of applications of OAM such as optical tweezers, laser material surface treatment, quantum entanglement, image processing, and quantum measurement as well as optical communication.[5]

Generation of the optical OAM beams is generally performed by using bulk free-space optics such as spiral phase plates, cylindrical lenses, spatial light modulators (SLMs) and so on.[6] On the other hand, fiber based OAM beam generation methods would be compact and low-loss when considering the optical fiber transmission. The fiber based generation

*E-mail: kishikawa.hiroki@tokushima-u.ac.jp

methods have been reported in literature such as multimode interference,[7] stress-induced phase difference,[8,9] effective index matching,[10,11] and acousto-optic interaction.[12,13] Among them, we focus on the acousto-optic (AO) effect for the interaction between the lightwave and the elastic wave due to the controllability and tunability.[14–17] The AO interaction has also been studied for optical switching of optical signals in a Bragg diffraction configuration.[18]

Optical mode conversion in optical fibers using AO effect has been reported in Refs.(19,20), in which the longitudinal or flexural mode is used as the elastic wave. Regarding OAM mode conversion, it is necessary to consider the matching of OAM between the incident optical beam and the elastic wave in addition to the conventional mode conversion. We employ an elastic vortex wave (EVW) which is generated by two orthogonal acoustical waves and possesses OAM on the elastic wave as suggested in[13] for this purpose. The analytical expression of the EVW, the strain and stress components, matching of phase and OAM should be revealed in order to understand the optical OAM mode conversion by using EVW. However, Ref.[13] did not describe the displacement and the phase profile of the EVW in the fiber. Although a few papers on AO coupling by EVWs have been reported,[19,20] only the contribution from a strain component S_{zz} has been reported, to the best of the authors knowledge. Therefore, in this paper, we derive the detailed analytical expression of the displacement and the phase profile of the EVW in the fiber. We also discuss the contribution of all the strain components and analyze the contribution to the perturbation of the dielectric constants induced by the strain for OAM mode conversion.[21] In addition, we reveal the power coupling between optical OAM modes and indicate the perfect coupling length in the squared graded index (GI) fiber.

This paper is organized as follows. Section 2 describes the detailed analytical expression of the displacement of the EVW, the strain and stress components, and the perturbation of the dielectric constants. Section 3 describes the Laguerre-Gaussian mode as an optical OAM beam. Section 4 analyzes the mode coupling using EVW for the OAM mode conversion. Finally, we present conclusion in Section 5.

2. Elastic vortex wave

We consider a GI optical fiber as shown in Fig.1. The radius of the fiber is b. The core region within radius a has a parabolic refractive index $n(r)$. In general, an ultrasonic wave propagating through an elastic medium is called elastic wave. Displacements in elastic waves are derived from the wave equations of motion. Considering a cylindrical coordinate system along the

optical fiber, the displacements $\boldsymbol{u}$ in the elastic wave are written as[22–24]

$$u_r = U(r) \begin{pmatrix} \sin(m\theta) \\ \cos(m\theta) \end{pmatrix} \exp[j(\Omega t - k_0 z)]$$

$$u_\theta = V(r) \begin{pmatrix} \cos(m\theta) \\ -\sin(m\theta) \end{pmatrix} \exp[j(\Omega t - k_0 z)]$$

$$u_z = W(r) \begin{pmatrix} \sin(m\theta) \\ \cos(m\theta) \end{pmatrix} \exp[j(\Omega t - k_0 z)], \tag{1}$$

where the radial variations are given by

$$U(r) = (A k_d J'_m(k_d r) + B k_0 J'_m(k_t r) + C \frac{m}{r} J'_m(k_t r))$$

$$V(r) = (A \frac{m}{r} J_m(k_d r) + B \frac{k_0 m}{k_t r} J_m(k_t r) + C J'_m(k_t r))$$

$$W(r) = -j(A k_0 J_m(k_d r) - B k_t J_m(k_t r)), \tag{2}$$

m is an integer describing the circumferential field variation, Ω is the angular frequency, k_0 is the propagation constant of the elastic wave, A,B,C are constants decided by boundary conditions, J_m is the Bessel function of the first kind, J'_m denotes its derivative with respect to the argument, and k_t and k_d are expressed as

$$k_t^2 = \Omega^2 / c_t^2 - k_0^2$$

$$k_d^2 = \Omega^2 / c_d^2 - k_0^2, \tag{3}$$

where the transverse wave velocity c_t and the bulk dilatational velocity c_d are given using the density ρ, Lame's constants λ and μ through

$$c_t^2 = \mu / \rho \tag{4}$$

$$c_d^2 = (\lambda + 2\mu) / \rho.$$

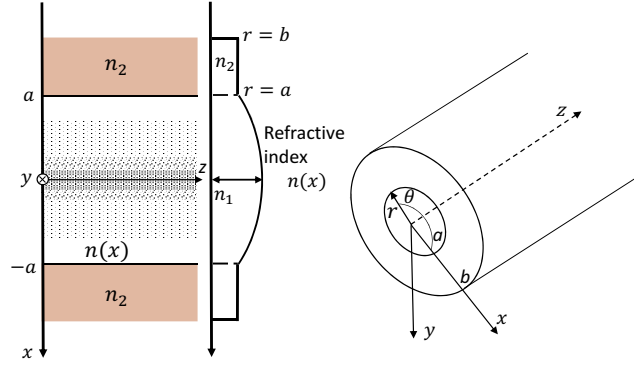We assume the elastic physical constants are uniform over the fiber cross section.

Fig. 1. Graded-index optical fiber.

The optical mode conversion is induced by the perturbation of optical fiber using elastic waves. Here, we derive strain and stress tensors from displacements $\boldsymbol{u}$ using Auld's notation. The strain tensor $\boldsymbol{S}$ is given by[22, 25]

$$\boldsymbol{S} = \begin{bmatrix} S_1 \\ S_2 \\ S_3 \\ S_4 \\ S_5 \\ S_6 \end{bmatrix} = \begin{bmatrix} S_{rr} \\ S_{\theta\theta} \\ S_{zz} \\ 2S_{\theta z} \\ 2S_{rz} \\ 2S_{r\theta} \end{bmatrix} = \begin{bmatrix} \frac{\partial u_r}{\partial r} \\ \frac{1}{r}(u_r + \frac{\partial u_\theta}{\partial \theta}) \\ \frac{\partial u_z}{\partial z} \\ \frac{\partial u_\theta}{\partial z} + \frac{1}{r}\frac{\partial u_z}{\partial \theta} \\ \frac{\partial u_r}{\partial z} + \frac{\partial u_z}{\partial r} \\ \frac{1}{r}\frac{\partial u_r}{\partial \theta} + \frac{\partial u_\theta}{\partial r} - \frac{u_\theta}{r} \end{bmatrix}. \tag{5}$$

The stress tensor $\boldsymbol{T}$ is derived from the strain tensor by

$$\boldsymbol{T} = \begin{bmatrix} T_1 \\ T_2 \\ T_3 \\ T_4 \\ T_5 \\ T_6 \end{bmatrix} = \begin{bmatrix} T_{rr} \\ T_{\theta\theta} \\ T_{zz} \\ T_{\theta z} \\ T_{rz} \\ T_{r\theta} \end{bmatrix}$$

$$= \begin{bmatrix} (\lambda + 2\mu)S_{rr} + \lambda S_{\theta\theta} + \lambda S_{zz} \\ \lambda S_{rr} + (\lambda + 2\mu)S_{\theta\theta} + \lambda S_{zz} \\ \lambda S_{rr} + \lambda S_{\theta\theta} + (\lambda + 2\mu)S_{zz} \\ 2\mu S_{\theta z} \\ 2\mu S_{rz} \\ 2\mu S_{r\theta} \end{bmatrix}. \tag{6}$$

Now, the dispersion relation of the elastic waves is derived using the boundary conditions

$T_{rr}, T_{rz}, T_{r\theta} = 0$ at $r = b$, where b is the fiber radius. The obtained dispersion relation is expressed by the following determinant.

$$\begin{vmatrix} m^2 - 1 - q_0^2(x-1) & m^2 - 1 - q_0^2(2x-1) & 2(m^2-1)[\gamma_m(q_t)-m] - q_0^2(2x-1) \\ \gamma_m(q_d) - m - 1 & \gamma_m(q_t) - m - 1 & 2m^2 - 2[\gamma_m(q_t)-m] - q_0^2(2x-1) \\ \gamma_m(q_d) - m & -(x-1)[\gamma_m(q_t)-m] & m^2 \end{vmatrix} = 0, \tag{7}$$

where $q_0 = k_0 b$, $q_t = k_t b$, $q_d = k_d b$, $x = \Omega^2/(k_0 c_t)^2$, and $\gamma_m(q) = q J_{m-1}(q)/J_m(q)$. The dispersion relation as shown in Fig.2 is obtained by solving eq.(7) by the bisection method. It reveals the relation between frequency f and phase velocity $c = \Omega/k_0$ of flexural waves.

In this figure, the 1st order flexural mode is the fundamental mode of flexural wave. The 2nd order and the 3rd order flexural modes are also plotted. The three lowest order modes are shown. In this research, we consider to use the fundamental mode of flexural wave for AO mode conversion. The group velocity of the fundamental mode of flexural wave c_g is calculated by

$$c_g = \frac{c}{1 - \frac{\omega}{c}\frac{\partial c}{\partial \omega}} \tag{8}$$

as shown in Fig. 3.
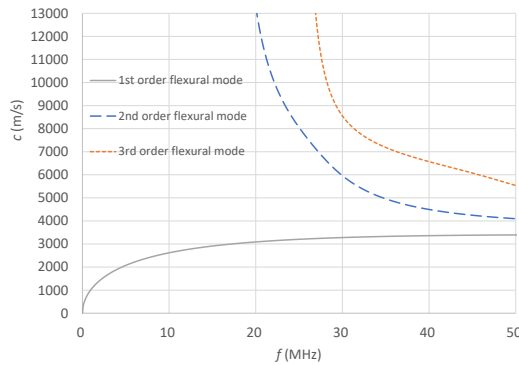
Fig. 2.   Dispersion relation of the guided flexural waves for $m=1$.
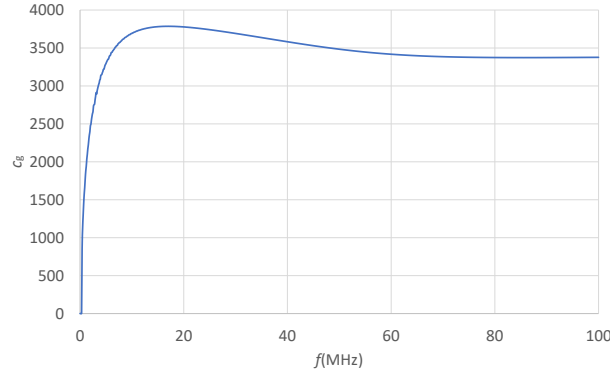
Fig. 3. Dispersion of group velocity c_g of the fundamental flexural mode.

The EVW is synthesized by orthogonalizing the x-axis component (upper set) and the y-axis component (lower set) of the displacements of eq.(1) with a phase difference of $\pi/2$ as

$$
\begin{aligned}
u_r &= U(r)\exp(jm\theta)\exp[j(\Omega t - k_0 z)] \\
u_\theta &= jV(r)\exp(jm\theta)\exp[j(\Omega t - k_0 z)] \\
u_z &= W(r)\exp(jm\theta)\exp[j(\Omega t - k_0 z)].
\end{aligned}
\tag{9}
$$

We assume physical parameters of silica, such as density $\rho = 2.2 \times 10^3 \text{kg/m}^3$, Lame's constants $\lambda = 1.6 \times 10^{10} \text{N} \cdot \text{m}^{-2}$, and $\mu = 3.1 \times 10^{10} \text{N} \cdot \text{m}^{-2}$. Examples of obtained displacements and phase profiles of EVW at f=0.3918 MHz are shown in Fig.4.

The acoustic power AP of the EVW in the fiber cross section is evaluated by eq.(10).[24]

$$
AP = 2\pi^2 \rho c_g f^2 \int_0^{2\pi} \int_0^b (|u_r|^2 + |u_\theta|^2 + |u_z|^2) r \, dr \, d\theta
\tag{10}
$$

The power of the EVW with $u_z^{max} = 50$nm is calculated to be 10.6mW. This power indicates the feasibility of the mode conversion in this setup because it is close to acousto-optic mode converter.[24] Therefore, we assume the maximum displacement is $u_z^{max} = 50$nm in this research.

It is found that the EVW has an OAM since the phase of the EVW is in a spiral shape. The displacements as a function of r are shown in Fig.5. The displacements u_r and u_θ distribute almost uniformly over the cross section. The displacement u_z, on the contrary, increases as r. The strain components caused by the EVW at $f = 0.3918$ MHz are shown in Fig.6. The strain $S_3(= S_{zz})$ increases with r and has the largest value around the fiber edge. The other components except for S_6 exist and are not negligible.
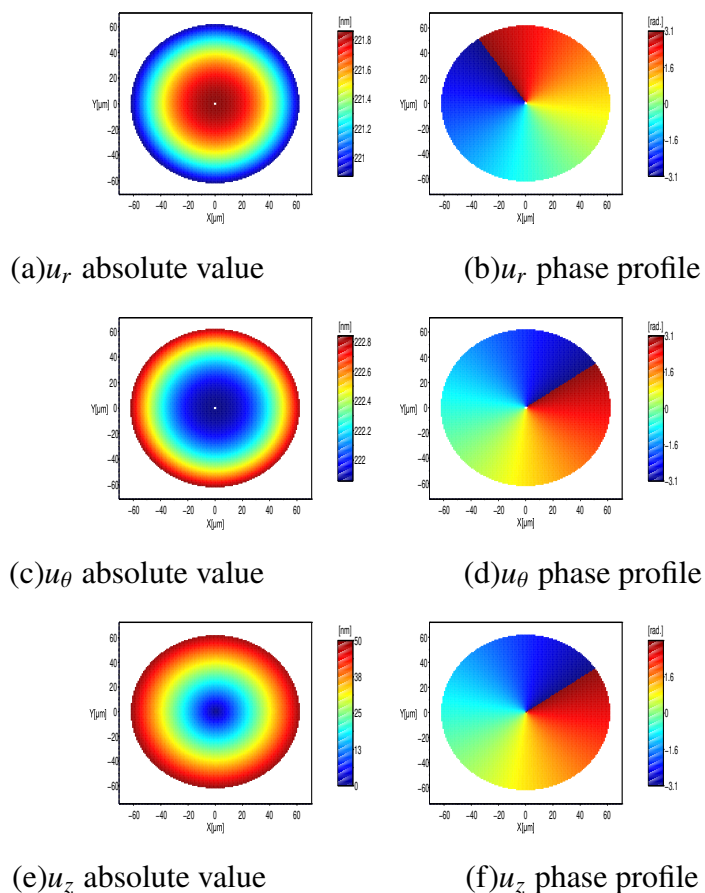
(a)u_r absolute value   (b)u_r phase profile

(c)u_θ absolute value   (d)u_θ phase profile

(e)u_z absolute value   (f)u_z phase profile

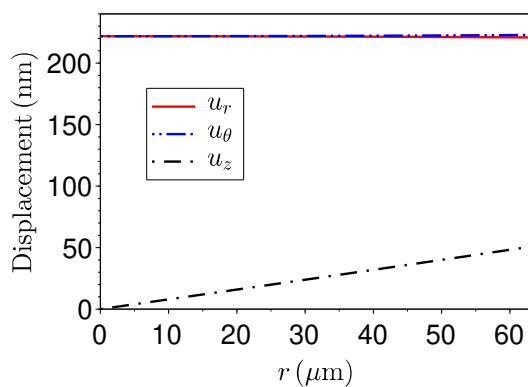**Fig. 4.** Absolute value and phase profile of EVW at f=0.3918MHz.

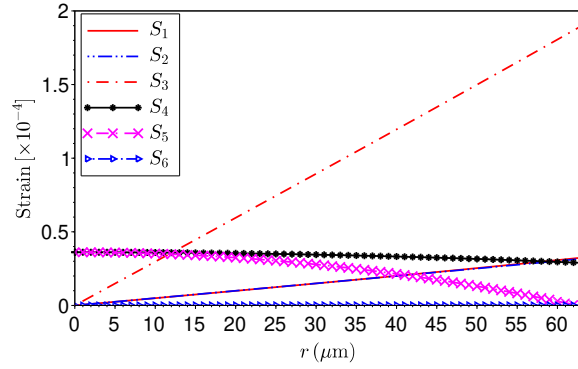**Fig. 5.** Absolute value of displacement at f=0.3918 MHz.

Fig. 6. Distribution of the strain components at f=0.3918 MHz.

The perturbation of the dielectric constants induced by the elastic waves is obtained. The elasto-optic constants p_{ij} in silica of the fiber have the components $p_{11} = p_{22} = p_{33}, p_{12} = p_{13} = p_{21} = p_{23} = p_{31} = p_{32}$, and $p_{44} = p_{55} = p_{66}$. It is noted that $p_{44} = \frac{1}{2}(p_{11} - p_{12})$.[26, 27] The perturbation of the dielectric constants $\Delta\varepsilon$ due to the acousto-optic interaction is given by the tensor notation as[26–28]

$$
\Delta\varepsilon =
\begin{bmatrix}
\Delta\varepsilon_1 \\
\Delta\varepsilon_2 \\
\Delta\varepsilon_3 \\
\Delta\varepsilon_4 \\
\Delta\varepsilon_5 \\
\Delta\varepsilon_6
\end{bmatrix}
=
\begin{bmatrix}
\Delta\varepsilon_{rr} \\
\Delta\varepsilon_{\theta\theta} \\
\Delta\varepsilon_{zz} \\
\Delta\varepsilon_{z\theta} \\
\Delta\varepsilon_{rz} \\
\Delta\varepsilon_{r\theta}
\end{bmatrix}
$$

$$
= -\varepsilon_0\varepsilon_r^2
\begin{bmatrix}
p_{11}S_1 + p_{12}S_2 + p_{12}S_3 \\
p_{12}S_1 + p_{12}S_2 + p_{12}S_3 \\
p_{12}S_1 + p_{12}S_2 + p_{11}S_3 \\
2p_{44}S_4 \\
2p_{44}S_5 \\
2p_{44}S_6
\end{bmatrix}.
$$

(11)

Here, ε_0 is the vacuum dielectric constant and ε_r is the relative dielectric constant of the fiber.

3. Optical OAM mode

We consider optical modes in the squared GI fiber. The refractive index $n(r)$ has the distribution given by

$$n^2(r) = \begin{cases} n_1^2[1 - (gr)^2] = n_1^2[1 - 2\Delta(r/a)^2] & r \leqq a \\ n_2^2 & r \geqq a, \end{cases} \tag{12}$$

where n_1 is the core center refractive index, n_2 is the cladding refractive index, $g = \sqrt{2\Delta}/a$ is the focusing constant, a is the fiber core radius, and Δ is the relative refractive index difference defined by $\Delta = (n_1^2 - n_2^2)/(2n_1^2)$. Maxwell's wave equation in the squared GI fiber is given by

$$\frac{\partial^2 E_y}{\partial r^2} + \frac{1}{r}\frac{\partial E_y}{\partial r} + \frac{1}{r^2}\frac{\partial^2 E_y}{\partial \theta^2} + [k^2 n_1^2(1 - g^2 r^2) - \beta^2]E_y = 0. \tag{13}$$

The mode electric field derived from this equation is called Laguerre-Gaussian (LG) mode[29, 30]

$$E_y(r, \theta) = E_{vn}e^{jv\theta}(r/w_0)^v L_n^{(v)}(r^2/w_0^2)e^{-\frac{1}{2}(r/w_0)^2}, \tag{14}$$

where $k = 2\pi/\lambda$, $\omega_0 = 1/\sqrt{kn_1 g}$ is called eigen spot size. $L_n^{(v)}$ is the associated Laguerre polynomial. The amplitude coefficient E_{vn} is expressed by

$$E_{vn} = \begin{cases} \sqrt{\dfrac{n}{2\pi(v+n)!w_0^2}} & (v = 0) \\ \sqrt{\dfrac{n}{\pi(v+n)!w_0^2}} & (v \geqq 1). \end{cases} \tag{15}$$

The propagation constant of this LG mode is given by

$$\beta = \sqrt{k^2 n_1^2 - 2kn_1^2 g(2n + v + 1)}$$
$$\cong kn_1 - (2n + v + 1)g \tag{16}$$

where n is the radial index corresponding to the node order of the LG mode, and v is the azimuthal index called topological charge.

The core center refractive index n_1 and the cladding refractive index n_2 of the squared GI fiber is assumed as 1.46 and 1.45, respectively. The core diameter $2a$ is 62.5μm and the cladding diameter $2b$ is 125μm. The optical incident wavelength is $\lambda_c = $ 1550nm. The equivalent index of refraction β/k with respect to the radius a of the core is shown in Fig.7 for $N = 2n + v$. Hereafter, Laguerre-Gaussian (LG) mode is expressed as LG_{vn}. Figs.8-10 show mode profiles of the lowest three modes. LG_{00} is a general Gaussian beam as shown in Fig.8. In contrast, the phase of the LG modes with v=1 in Fig.9 and v=2 in Fig. 10 are in spiral shapes. From these spiral phases it is found that the LG modes for $v \geqq 1$ carry OAM.
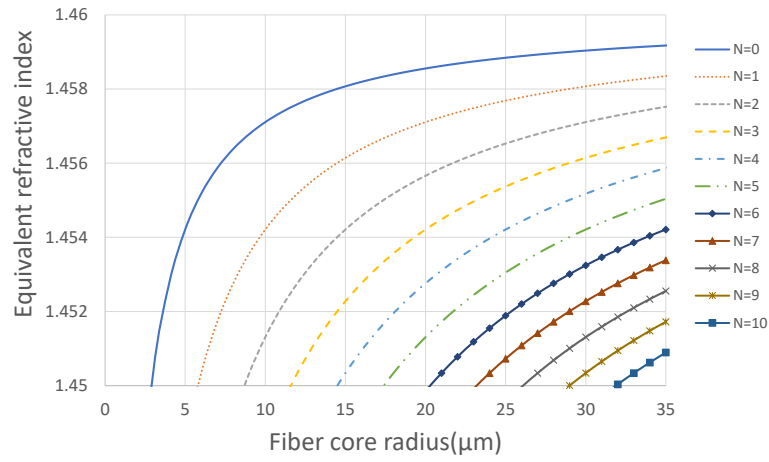
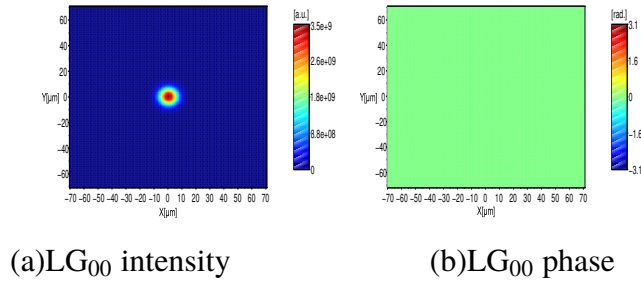**Fig. 7.**   Equivalent refractive index vs. core radius.

(a)LG$_{00}$ intensity   (b)LG$_{00}$ phase

Fig. 8.   Intensity and phase profile of LG$_{00}$.

(a)LG$_{10}$ intensity   (b)LG$_{10}$ phase
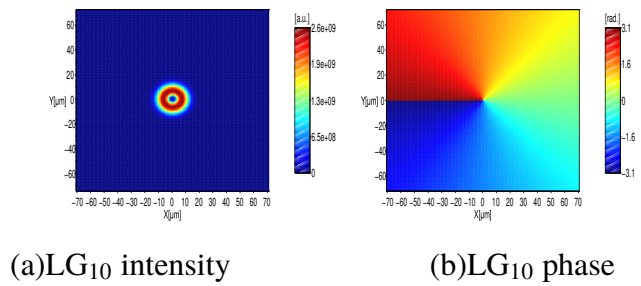
Fig. 9.   Intensity and phase profile of LG$_{10}$.

(a)LG_{20} intensity   (b)LG_{20} phase
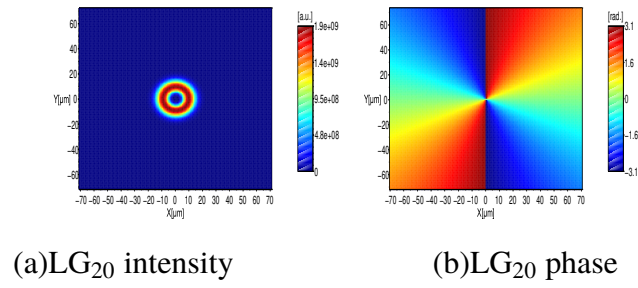
Fig. 10.   Intensity and phase profile of LG_{20}.

4.   AO Mode Conversion Theory

4.1   Phase matching condition

We consider the phase matching condition for AO coupling between LG modes and EVW. The phase matching condition of the propagation constants is given by[20, 31–33]

$$\beta_l - \beta_p = k_0, \tag{17}$$

where β_l and β_p are the propagation constants of input and output optical modes, respectively, and k_0 is the propagation constant of EVW. From eq.(15), the velocity of the EVW required for efficient AO coupling is found to be

$$c = 2\pi f / (\beta_l - \beta_p). \tag{18}$$

We can specify the frequency and phase velocity of the EVW for optical mode conversion from this phase matching condition for optical LG_{00} and LG_{10} as shown in Fig.11. The solid curve indicates the relation of phase velocity c and frequency f of the EVW. The dashed line corresponds to $2\pi/(\beta_1 - \beta_2)$, where β_1 and β_2 are the propagation constants LG_{00} and LG_{10} modes, respectively. The frequency of the elastic wave satisfying the phase matching condition is obtained at the cross point of the solid curve and the dashed line, which is found to be 0.3918 MHz. Similarly, the frequency for AO coupling between LG_{10} and LG_{20} is obtained at 0.3925 MHz.
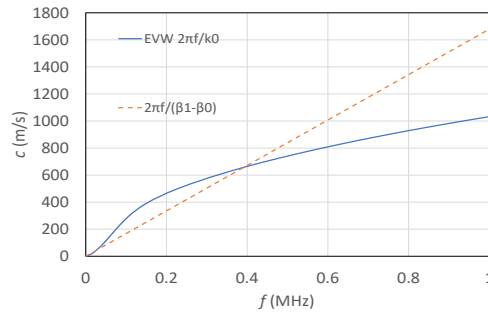
Fig. 11. Phase matching condition between LG_{00} and LG_{10}.

4.2   OAM mode coupling

The mode coupling equation is derived from Maxwell's wave equation. Electro magnetic waves are expressed by superposition of all optical modes propagated in the optical waveguide as[20, 34]

$$E(r, \theta, z) = \sum_p \frac{F_p(r, \theta)}{N_p} \mathcal{A}_p(z) e^{-j(\beta_p z - \omega t)}$$

$$H(r, \theta, z) = \sum_p \frac{G_p(r, \theta)}{N_p} \mathcal{B}_p(z) e^{-j(\beta_p z - \omega t)}, \tag{19}$$

where $\mathcal{A}_p(z)$ and $\mathcal{B}_p(z)$ are the complex amplitudes, $F_p(r, \theta)$ and $G_p(r, \theta)$ are the transverse distributions of the electric and magnetic field for the mode p, N_p is a normalization coefficient, and ω is the angular frequency of the optical mode. Here, we adopt normalization to optical power as

$$\int \int [F_p^*(r, \theta) \times G_l(r, \theta) + F_p(r, \theta) \times G_l^*(r, \theta)] \cdot e_z r \, dr \, d\theta$$
$$= 4\delta_{pl} N_p^2, \tag{20}$$

where δ_{pl} represents the Kronecker delta and e_z is the unit vector to z direction. $\mathcal{A}_p(z)$ and $\mathcal{B}_p(z)$ are expressed as

$$\mathcal{A}_p(z) = c_p^+(z) e^{-j\beta_p^+ z} + c_p^-(z) e^{-j\beta_p^- z}$$

$$\mathcal{B}_p(z) = c_p^+(z) e^{-j\beta_p^+ z} - c_p^-(z) e^{-j\beta_p^- z}. \tag{21}$$

Mode coupling equations are derived from these notations and Maxwell's equations as

$$\frac{dc_p^+(z)}{dz} = \sum_{l=0}^{q} c_l^+(z)\vartheta_{pl}^{++} e^{j(\beta_p - \beta_l - k)z} e^{j\Omega t}$$

$$+ c_l^-(z)\vartheta_{pl}^{+-} e^{j(\beta_p + \beta_l - k)z} e^{j\Omega t}$$

$$\frac{dc_p^-(z)}{dz} = \sum_{l=0}^{q} c_l^-(z)\vartheta_{pl}^{--} e^{j(\beta_p - \beta_l - k)z} e^{j\Omega t}$$

$$+ c_l^+(z)\vartheta_{pl}^{-+} e^{j(\beta_p + \beta_l - k)z} e^{j\Omega t}.$$

(22)

These two equations consider all optical modes, both forward waves and backward waves. However, only the optical modes satisfying the phase matching condition are able to transfer energy between optical modes. For simplicity, the backward waves are not considered in this mode coupling. In addition, the time dependent terms are excluded since the velocity of light is much faster than that of elastic waves. Thus, the mode coupling equations are simplified as[20]

$$\frac{d\mathcal{A}_p(z)}{dz} = \sum_{l=0}^{q} \mathcal{A}_l(z)\vartheta_{pl} e^{j(\beta_p - \beta_l - k)z},$$

(23)

where ϑ_{pl} is called coupling coefficient. It is expressed by[34–39]

$$\vartheta_{pl} = \frac{\omega}{2(\beta_l - \beta_p)} \int \int \frac{F_p(r,\theta) \cdot F_l^*(r,\theta)}{N_p N_l} \frac{d\varepsilon}{dz} r dr d\theta,$$

(24)

where $d\varepsilon/dz$ indicates the change amount of the dielectric constant by elastic waves. $\varepsilon(r,\theta,z)$ is the total dielectric constant including the perturbation term $\Delta\varepsilon(r,\theta,z)$ induced by elastic waves

$$\varepsilon(r,\theta,z) = \varepsilon_u + \Delta\varepsilon(r,\theta,z),$$

(25)

where ε_u is the unperturbed dielectric constant. Finally, the amount of change in z direction is expressed by the following equation because $\Delta\varepsilon(r,\theta,z)$ is derived from displacements expressed by eq.(9) in the form of $R(r)e^{jm\theta}e^{-jk_0 z}$,

$$\frac{d\varepsilon}{dz} = -jk_0\Delta\varepsilon(r,\theta,z).$$

(26)

The OAM matching condition should be satisfied when considering OAM mode conversion by EVW in addition to the phase matching condition. For example, a mode conversion from LG_{00} to LG_{20} is not achieved by using an EVW at $m=1$. This is because the OAM matching is not satisfied. To execute the mode conversion from LG_{00} to LG_{20}, an EVW at $m = 2$ has to

be used. This matching condition is given by

$$\text{OAM}_{v,n} = \text{OAM}_{v-m,n} + \text{EVW}_{m,n}. \tag{27}$$

We show a set up for the OAM mode conversion using EVW in Fig.12. Two shear-mode piezoelectric transducers (PZTs) are stacked so that their vibration directions are perpendicular to each other.[13] They are oscillated with $\pi/2$ phase difference to generate an EVW. There is a hole in the central area of the PZTs to pass through the input fiber. The OAM lightwave is coming from the input fiber and incident into the stripped fiber. Here, the stripped fiber is an unjacketed fiber. The PZTs are connected to the stripped fiber by a horn to excite the EVW onto the stripped fiber. Then, the OAM mode conversion is achieved in the stripped fiber.
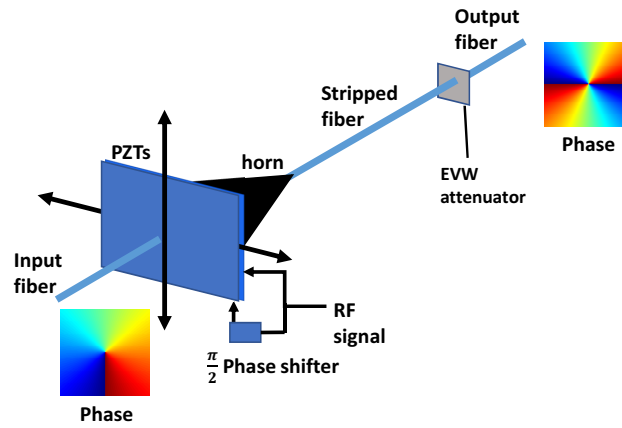

Fig. 12.   Schematic diagram of the OAM mode conversion setup.

4.3   AO mode coupling result

We describe calculated results using the mode coupling equation. As examples, we consider mode conversion from LG_{00} to LG_{10} and from LG_{10} to LG_{20}. We use EVWs at $f=0.3918$ MHz (between LG_{00} and LG_{10}) and $f=0.3925$ MHz (between LG_{10} and LG_{20}) that satisfy the phase matching condition. Maximum displacement of the EVWs is $u_z^{max}=50$nm. Here, $p_{11} = 0.121, p_{12} = 0.270, p_{44} = -0.0745$. The calculated coupling coefficient ϑ_{pl} and perfect coupling length CL are tabulated in Table I. Contribution of $\Delta\varepsilon_1$ and $\Delta\varepsilon_2$ are relatively large among the 6 coefficients for both cases. Fig.13 shows the coupling mode power as a function of z. We confirm the OAM mode conversion using the EVWs in the squared GI fiber from these results. The OAM mode conversion from LG_{00} to LG_{10} is achieved at the propagation distance about 34 mm as shown in Fig.13(a). It is found from Table I that $\Delta\varepsilon_1, \Delta\varepsilon_2, \Delta\varepsilon_3, \Delta\varepsilon_4$, and $\Delta\varepsilon_5$ contribute to the OAM mode conversion. Similarly, the OAM mode conversion from LG_{10} to

LG_{20} is achieved at the propagation distance about 23 mm as shown in Fig.13(b). It is also found from Table I that $\Delta\varepsilon_1, \Delta\varepsilon_2, \Delta\varepsilon_3, \Delta\varepsilon_4$, and $\Delta\varepsilon_5$ except for $\Delta\varepsilon_6$ contribute to the OAM mode conversion.

The perturbation of the dielectric constants may be different for desired OAM mode conversions and conditions. Thus, revealing such perturbation characteristics would provide studies for selectively exciting elastic waves having strong contribution to OAM mode conversions. It leads to optimize the elastic wave power and improve the mode conversion efficiency.

Table I. Absolute value of coupling coefficient ϑ_{pl} and perfect coupling length CL.

$|\vartheta_{01}|$	45.7	$|\vartheta_{12}|$	66.2	CL_{01}	34mm	CL_{12}	23mm
$|\vartheta_{\Delta\varepsilon_1}|$	25.9	$|\vartheta_{\Delta\varepsilon_1}|$	36.3	$CL_{\Delta\varepsilon_1}$	60mm	$CL_{\Delta\varepsilon_1}$	42mm
$|\vartheta_{\Delta\varepsilon_2}|$	22.8	$|\vartheta_{\Delta\varepsilon_2}|$	31.9	$CL_{\Delta\varepsilon_2}$	52mm	$CL_{\Delta\varepsilon_2}$	45mm
$|\vartheta_{\Delta\varepsilon_3}|$	3.92	$|\vartheta_{\Delta\varepsilon_3}|$	5.48	$CL_{\Delta\varepsilon_3}$	400mm	$CL_{\Delta\varepsilon_3}$	290mm
$|\vartheta_{\Delta\varepsilon_4}|$	15.1	$|\vartheta_{\Delta\varepsilon_4}|$	15.8	$CL_{\Delta\varepsilon_4}$	100mm	$CL_{\Delta\varepsilon_4}$	100mm
$|\vartheta_{\Delta\varepsilon_5}|$	14.9	$|\vartheta_{\Delta\varepsilon_5}|$	15.4	$CL_{\Delta\varepsilon_5}$	100mm	$CL_{\Delta\varepsilon_5}$	100mm
$|\vartheta_{\Delta\varepsilon_6}|$	0.014	$|\vartheta_{\Delta\varepsilon_6}|$	0.019	$CL_{\Delta\varepsilon_6}$	around 100m	$CL_{\Delta\varepsilon_6}$	around 100m
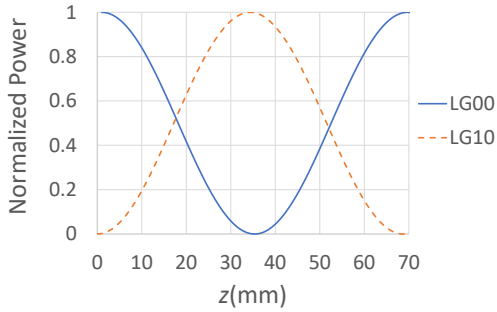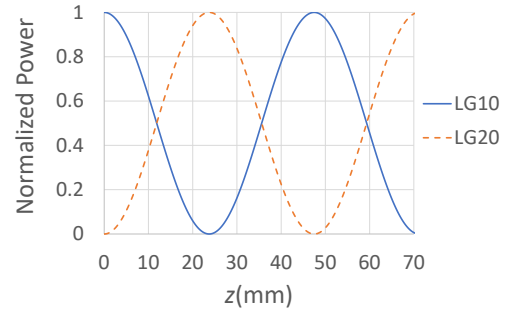
(a)Between LG_{00} and LG_{10} (b)Between LG_{10} and LG_{20}

Fig. 13. Coupling between LG_{00} and LG_{10}, between LG_{10} and LG_{20} considering all the perturbation components.

5. Conclusion

In this paper, we theoretically discussed optical OAM mode conversion using EVW in the squared GI fiber. The detailed analytical expression of the displacement and the phase profile of the EVW was clarified. Numerical calculation results revealed that 5 components of the

perturbation of the dielectric constant contributed to the mode coupling. We assumed 50nm as the EVW amplitude in this research. The amplitude of the elastic wave is related to the mode conversion efficiency. For that reason, the perfect mode conversion distance is controllable by changing the EVW amplitude.

References

1) N. Bozinovic, Y. Yue, Y. Ren, M. Tur, P. Kristensen, H. Huang, A. E. Willner, S. Ramachandran, Science **340**, 1545 (2013)

2) S. Ramachandran, P. Kristensen, Nanophotonics **2**, 455 (2013)

3) M. P. J. Lavery, A. J. robertson, A. sponselli, J. Courtial, N. K. Steinhoff, G. A. Tyler, A. E. Willner and M. J. Padgett, New J. Phys. **15**, 13024 (2013)

4) A. E. Willner, Y. Ren, H. Huang, Y. Yan, N. Ahmed, G. Xie, J. Wang, Y. Yue, M. P. J. Lavery, M. Tur, M. J. Padgett, S. Ramachandran, N. Bozinovic, and L. Li, IEEE Photonics Society Newsletter **28**, 12 (2014)

5) B. Sephton, A. Dudley, and A. Forbes, "Revealing the radial modes in vortex beams," Appl. Opt. **55**, 7830 (2016).

6) A. E. Willner, H. Huang, Y. Yan, Y. Ren, N. Ahmed, G. Xie, C. Bao, L. Li, Y. Cao, Z. Zhao, J. Wang, M. P. J. Lavery, M. Tur, S. Ramachandran, A. F. Molisch, N. Ashrafi, and S. Ashrafi, Advances in Optics and Photonics **7**, 66 (2015)

7) J. Zhou, Opt. Express **23**, 10247 (2015).

8) D. McGloin, N. B. Simpson, and M. J. Padgett, Appl. Opt. **37**, 469 (1998).

9) N. Bozinovic, S. Golowich, P. Kristensen, and S. Ramachandran, Opt. Lett. **37**, 2451, (2012).

10) Y. Yan, L. Zhang, J. Wang, J. Y. Yang, I. M. Fazal, N. Ahmed, A. E. Willner, and S. J. Dolinar, Opt. Lett. **37**, 3294 (2012).

11) Y. Han, Y. G. Liu, W. Huang, Z. Wang, J. Q. Guo, and M. M. Luo, Opt. Express **24**, 17272 (2016).

12) W. Zhang, K. Wei, L. Huang, D. Mao, B, Jiang, F. Gao, G. Zhang, T. Mei, and J. Zhao, Opt. Express **24**, 19278 (2016).

13) P. Z. Dashti, F. Alhassen, H. P. Lee, Phys. Rev. Lett. **96**, 43604 (2006)

14) N. Goto, Y. Miyazaki and Y. Akao, Trans. IEICE Japan **66**, 442 (1983)

15) N. Goto, Y. Miyazaki, IEEE J. on Selected Areas in commun. **8**, 1160 (1990)

16) N. Goto, Y. Miyazaki, Jpn. J. Appl. Phys. **38**, 3179 (1999)

17) N. Goto, Y. Miyazaki, Jpn. J. Appl. Phys. **50**, 72503 (2011)

18) S. Kakio, S. Uotani, M. Kitamura, Y. Nakagawa, T. Hara, H. Ito, T. Kobayashi, and M. Watanabe, Jpn. J. Appl. Phys. **46**, 4608 (2007)

19) W. Zhang, L. Huang, K. Wei, P. Li, B. Jiang, D. Mao, F. Gao, T. Mei, G. Zhang, and J. Zhao, Opt. Express **24**, 10376 (2016)

20) G. M. Fernandes, N. J. Muga, A. N. Pinto, J. Lightwave Technol. **32**, 3257 (2014)

21) T. Shoro, H. Kishikawa, N. Goto, Proceeding of Symposium on Ultrasonic Electronics, 1P1-3 (2018)

22) B. A. Auld, Acoustic fields and waves in solids volume I (Krieger publishing company, Florida, 1973) 2nd ed., p.358

23) R. N. Thurston, J. Acoust. Soc. Am. **64**, 1 (1978)

24) H. E. Engan, B. Y. Kim, J. N. Blake, H. J. Shaw, J. Lightwave Technol. **6**, 428 (1988)

25) B. A. Auld, Acoustic fields and waves in solids volume II, (Krieger publishing company, Florida, 1973) 2nd ed., p.104

26) J. Xu, R. Stroud, Acousto-Optic Devices:Principles, Design, and Applications (John Wiley & Sons, Inc, New York, 1992), p.47

27) A. Yariv, P. Yeh, Optical waves in crystals (Willey Interscience Publication, New York, 1984) p.177

28) K. Yamanouchi, K. Higuchi, K. Shibayama, Appl. Phys. Lett. **28**, 75 (1976)

29) H. G. Unger, Planar optical waveguides and fibers Oxford Engineering Science Series (Clarendon press, Oxford, 1977), p.552

30) M. J. Adams, An introduction to optical waveguides (John Wiley & Sons Ltd., Chichester ,1981) p.290

31) D. Östling, H. E. Engan, Opt. Lett. **20**, 1247 (1995)

32) H. S. Kim, S. H. Yun, I. K. Kwang, and B. Y. Kim, Opt. Lett. **22**, 1476 (1997)

33) Q. Li, X. Liu, H. P. Lee, IEEE Photonics Technol. Lett. **14**, 1551 (2002)

34) D. Marcuse, Theory of dielectric optical waveguides, (Academic Press, New York, 1974), p.95

35) E. H. Khoo, A. Q. Liu, X. M. Zhang, E. P. Li, J. Li, D. Pinjala, and B. S. Luk'yanchuk, Phys. Rev. B **80**, 35101 (2009)

36) T. Kondo, Y. Miyazaki and Y. Akao, Jpn. J. Appl. Phys. **17**, 1231 (1978)

37) J. N. Blake, B. Y. Kim, H. E. Engan, and H. J. Shaw, Opt. Lett. **12**, 281 (1987)

38) P. Z. Dashti, Q. Li, C. H. Lin, and H. P. Lee, Opt. Lett. **28**, 1403 (2003)

39) W. Zhang, L. Huang, K. Wei, P. Li B. Jiang, D. Mao, F. Gao, T. Mei, G. Zhang, and J. Zhao, Opt. Lett. **41**, 5082 (2016)